IEEE Access
Multidisciplinary | Rapid Review | Open Access Journal

Received June 3, 2020, accepted June 18, 2020, date of publication June 23, 2020, date of current version July 2, 2020.

*Digital Object Identifier 10.1109/ACCESS.2020.3004467*

# Enhancing MIMO Antenna Isolation Characteristic by Manipulating the Propagation of Surface Wave

**ZHUO YANG[1], JUN XIAO[2], AND QIUBO YE[2], (Senior Member, IEEE)**
[1]Navigation Institute, Jimei University, Xiamen 361021, China
[2]School of Information Engineering, Jimei University, Xiamen 361021, China

Corresponding author: Qiubo Ye (qbye@jmu.edu.cn)

This work was supported by Research Start-up Fund of Jimei University under Grant 4411/C618018.

**ABSTRACT** Multiple-input multiple-output (MIMO) antennas have been a mainstream technology in fifth generation (5G) communications. However, strong mutual coupling between both adjacent and nonadjacent elements is inevitable, especially among highly integrated devices. In this paper, a slit embedded mushroom electromagnetic bandgap structure (EBG) is primarily proposed to suppress the propagation of surface wave between antenna elements. Subsequently, complementary split-ring resonators (CSRRs) are periodically arranged in two sides of the ground to steer the surface wave. By effectively utilizing the unusual electromagnetic property of EBG and CSRR to manipulate the propagation of surface wave, the mutual coupling between antenna elements has immensely alleviated. Finally, an H-shape defected ground structure (DGS) is introduced to reinforce decoupling effect. In order to validate the feasibility of the design principle, a prototype of the proposed antenna has been fabricated and measured. Measured results demonstrate that the decoupling concept in this paper is reasonable and approximately 12 dB reduction of mutual coupling is realized.

**INDEX TERMS** Multiple-input multiple-output (MIMO), mutual coupling, slit embedded electromagnetic bandgap structure (EBG), complementary split-ring resonator (CSRR).

## I. INTRODUCTION

Nowadays, with the rapid development of wireless communication systems, multiple-input multiple-output (MIMO) antennas have been a vital part in fifth generation (5G) communications, owing to its intrinsic advantages of high transmission rate, large channel capacity and immunity to the multiple path loss [1]. More antenna elements with small spacing (less than a half wavelength) have been a mainstream in 5G small station construction, so the remaining space for antenna placement is gradually narrowed. It is indisputable that the mutual coupling between antenna elements can't be negligible in MIMO antenna design when antenna elements are arranged compactly, which will deteriorate the comprehensive performance of MIMO antennas, inclusive of reliable channel capacity, low spatial correlation and the high signal-to-interference-pulse-noise-ratio [2]. Consequently, antenna elements decoupling has been considered as an efficient way to improve the comprehensive ability of systems.

The associate editor coordinating the review of this manuscript and approving it for publication was Masood Ur-Rehman.

Varieties of techniques have been demonstrated for MIMO antenna decoupling. For instance, the simple way to increase the isolation between antenna elements is to utilize neutralization line (NL) [3] or decoupling network [4] as the decoupling circuit to connect antenna elements. When the decoupling current in interconnector cancels with the coupling current between antenna elements, the high isolation will be achieved. However, the above techniques have a common deficiency that the decoupling circuit as interconnector will inevitably increase the difficulty of impedance match and introduce extra insertion loss which will decrease antenna efficiency. The mutual coupling is mainly derived from the propagation of surface wave when multiple antennas share the common ground plane. Hence, another simple way to enhance antenna elements isolation is applying defected ground structure (DGS) [5]–[7], which can effectively interrupt the propagation of surface wave among antenna elements to eradicate the mutual coupling. Unfortunately, the DGS suffers from the drawback of high front to back ratio. Another design concept for isolation improvement is utilizing the intrinsic high isolation of antenna elements rather than inserting decoupling structure. Prevailing decoupling approaches

based on this concept include that orthogonal polarization [8], [9] and pattern diversity [10], [11], which have a distinguishing advantage that no extra space is needed to place decoupling structure with achieving complementary radiation patterns or polarizations simultaneously. But these decoupling techniques have a rigorous requirement for antenna elements design and arrangement, which restrict MIMO antennas in some practical applications. Most recently, various studies on metastructure provide a new insight to attain high isolation performance. It is well known that metamaterials are three dimensional (3D) and metasurfaces are two dimensional (2D), respectively. Both consist of artificially designed subwavelength periodic unit and have a unique electromagnetic property that controls the propagation and polarization of electromagnetic waves [12], [13]. In [14], a novel dual band split planar electromagnetic bandgap (EBG) has been proposed, which consists of a dense array of metallic patches whose edges are connected to the adjacent one through a thin meander-line metallic strip. After utilizing EBG to hinder the propagation of surface wave, the mutual coupling has been tremendously alleviated. Another decoupling concept of metastructure has been proposed in [15], the metasurface superstrate is utilized as a polarization converter for surface wave coupling mode. When surface wave coupling mode is orthogonal with antenna element resonant mode, the low correlation of antenna elements can be attained.

In this paper, a high isolation two-element MIMO antenna has been proposed and analyzed, which works at 3.25 GHz and is suitable for the 5G frequency band (sub-6 GHz) [16]. The two rectangular patch antennas are chosen as antenna elements due to its inherent advantages of low profile, low cost and ease of fabrication. The design guidelines and detailed analysis of microstrip patch antenna can be viewed in [17]. A novel interdigital slit embedded mushroom EBG has been inserted between antenna elements with the aim of suppressing the propagation of surface wave. Moreover, complementary split-ring resonators (CSRRs) and the H-shape defected ground structure (HDGS) have been deposited in ground adjacent to antenna edges for enhancing decoupling effect. After the above operations have been implemented, approximately 12 dB reduction of mutual coupling is realized.This paper is organized as follows. The antenna configuration, design procedures and working mechanism are described in section II. In section III, the measured results of the fabricated antenna are presented and discussed. A conclusion is briefly summarized in section IV, while the performance and comparison are also discussed.

## II. ANTENNA DESIGN AND ANALYSIS

### A. ANTENNA CONFIGURATION

Fig. 1 elaborately depicts the configuration of the proposed high isolation MIMO antenna, which is printed on the rectangular FR4 substrate material ($\varepsilon_r = 4.4, \tan\delta = 0.02.$) with the thickness of 3 mm and the dimension of 70∗40 mm$^2$. The two

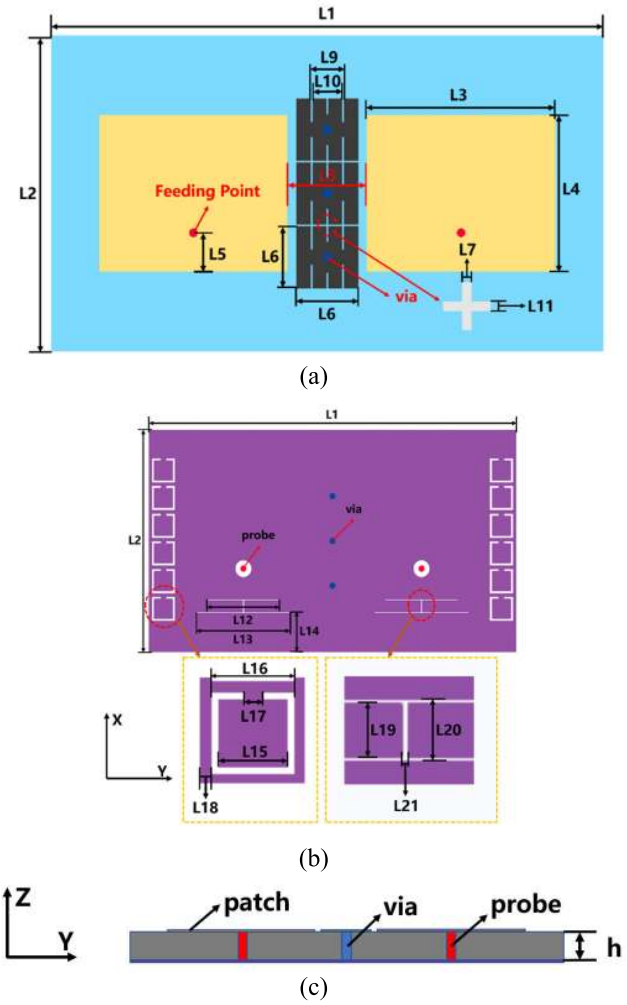


**FIGURE 1.** Geometry of the proposed antenna. (a) Top view. (b) Bottom view. (c) Side view.

port H-plane coupled array consists of two rectangular patch antenna elements which are identical and symmetrically placed on the top layer of FR4 substrate with the distance of edge to edge 10mm. The EBG structure is inserted between the gap of antenna elements nonradiation edges, which is constituted by periodic interdigital slit embedded mushroom patches grounded by metal vias with the diameter of 1mm. Antenna elements share a common ground which is located in the bottom layer of substrate. Moreover, CSRRs are etched in the ground two sides adjacent to the nonradiation edges of antenna elements. In addition, HDGSs are at the position which adjacent to the radiation edge of antenna elements. The antenna elements are fed from 50Ω input ports behind the ground plane. In this design, a full wave electromagnetic simulation software high-frequency structure simulator (HFSS) is used to analyze and optimize the proposed antenna, whose final dimensions are listed in Table 1.

### B. ANTENNA DESIGN PRECEDURES

For illustrating the detailed design procedures of the proposed MIMO antenna, the evolution of the proposed MIMO antenna

**TABLE 1. Geometrical sizes of the proposed antenna.**

| Parameters | $L_1$ | $L_2$ | $L_3$ | $L_4$ | $L_5$ | $L_6$ | $L_7$ | $L_8$ |
|---|---|---|---|---|---|---|---|---|
| Value(mm) | 70 | 40 | 24 | 20 | 4.8 | 8 | 0.1 | 10 |
| Parameters | $L_9$ | $L_{10}$ | $L_{11}$ | $L_{12}$ | $L_{13}$ | $L_{14}$ | $L_{15}$ | $L_{16}$ |
| Value(mm) | 3.9 | 4.1 | 0.1 | 14 | 18 | 7 | 3.5 | 4.5 |
| Parameters | $L_{17}$ | $L_{18}$ | $L_{19}$ | $L_{20}$ | $L_{21}$ | $h$ | | |
| Value(mm) | 0.9 | 0.3 | 2 | 2.6 | 0.3 | 3 | | |

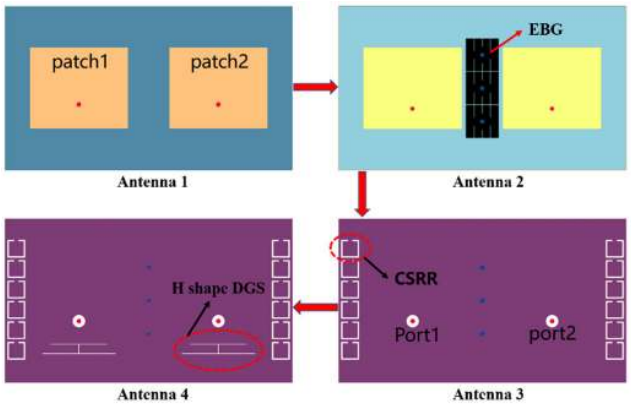


**FIGURE 2. The evolution of proposed antenna.**

has been elaborately depicted in figure 2. For simplicity, the four arrays in antenna design procedures are expressed as antenna 1, antenna 2, antenna 3, and antenna 4 in following sections, respectively. Initially, a two element H-plane coupled array has been designed in antenna 1 without any decoupling structure. Secondly, the slit integrated mushroom EBG structures have been periodically placed between the antenna elements in antenna 2. Thirdly, the CSRR structures have been periodically etched in the two sides of antenna ground in antenna 3. Finally, the H shape DGS structures have been introduced in antenna 4, which will generate decoupling current to neutralize the coupling current of antenna elements for enhancing isolation. Subsequently, the proposed high isolation MIMO antenna is achieved.

### C. DECOUPLING CONCEPT

As mentioned in previous section, the mutual coupling of antenna elements is mainly derived from the propagation of surface wave. According to the electromagnetic (EM) wave propagation theory, the corresponding y-component of electric filed related to surface wave travelling along the +y direction can be expressed as follows [18]:

$$E(y,t) = E_0 e^{jky}.e^{jwt} \quad (1)$$

$$\mathrm{k} = \omega.\sqrt{\mu\varepsilon} \quad (2)$$

In formula (1), assuming the time convention $e^{jwt}$, $E_0$ is the amplitude of the surface wave. k is wavenumber in media which can be expressed in formula (2), $\omega$ is angular frequency of travelling wave, $\mu$ is effective permeability of media and $\varepsilon$ is effective permittivity related to media, respectively. It is indisputable that both permeability and permittivity are positive in natural electromagnetic media, so the wavenumber k is real number that EM wave can normally travel. Conversely, the negative effective permeability and permittivity can be achieved in artificial periodic structures at definite resonant frequency. A material shows either negative permeability [19] or permittivity [20] characterized as single-negative (SNG) metamaterial, which corresponds to wavenumber k being imaginary number. Hence, the EM wave will evanescent dramatically when it propagates in SNG metamaterial. Besides, double-negative (DNG) metamaterials exhibit negative permeability and permittivity simultaneously [21]. Intriguingly, despite the fact that wavenumber k associated with DNG metamaterial is real number, the EM wave energy will be reflected when it travels in DNG metamaterial, which is due to the exclusive back-wave propagation property of DNG metamaterial [22]. In short, the surface wave between antenna elements can be immensely suppressed by effectively using the unusual electromagnetic property of metamaterial.

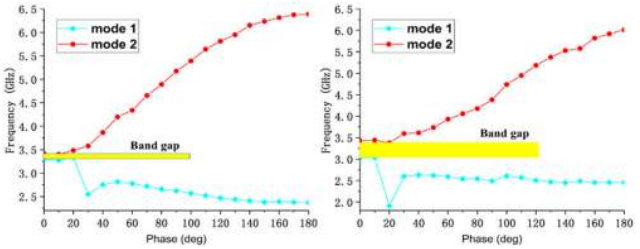


**FIGURE 3. The dispersion diagrams of EBG structures along Y direction: without interdigital slits (left) and with interdigital slits (right).**

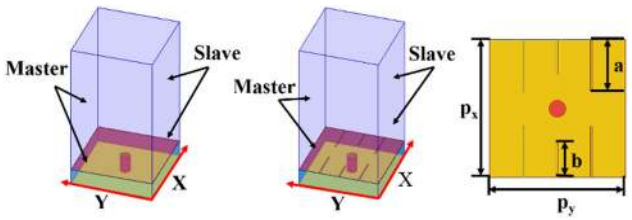


**FIGURE 4. Eigenmode simulation model for unit cell: $p_x = p_y = 8.05$ mm, a = 3 mm, b = 2 mm.**

EBG, a branch of metamaterial, is derived from the photonic band gap (PBG) and can be constituted by 2D/ 3D periodic metal or the mixture concerning about metal and dielectric components [23], [24]. There are two distinguishing features of EBG that can achieve in phase reflection and surface wave suppression. The in phase reflection property is usually utilized for antenna gain improvement and the feature of surface wave suppression can be applied for MIMO decoupling, respectively. In this paper, a novel slit combined with mushroom like EBG structure is employed to suppress the surface wave travelling between antenna elements, which is the evolution of conventional mushroom like EBG integrated with interdigital slit ingeniously. The dispersion diagrams of designed interdigital slit embedded mushroom EBG and conventional mushroom EBG are carried out by HFSS eigenmode solver and exhibited in figure 3. As shown in figure 4, two pairs of master and slave boundary condition

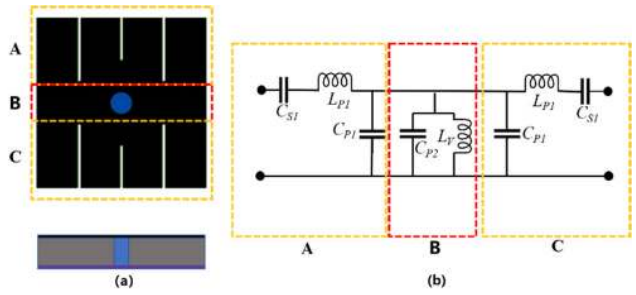


**FIGURE 5.** (a) Three sections of the physical model. (b) 1-D equivalent circuit model of EBG structure.

are applied in X and Y direction for simulating unit cell of EBG. From results with and without interdigital slit presented simultaneously for comparison, it can be seen clearly that the original stop band is broadened after the insertion of interdigital slit, which can be attributed to the additional capacitance introduced by the interdigital slit resulting in the wide bandstop response [25]. To further illustrate the bandstop characteristic of the slit embedded EBG, the physical model of EBG and corresponding generic 1-D equivalent circuit model are shown in figure 5, which has been divided into three sections from A to C for qualitative analysis conveniently and better understanding the design scheme. In section A, $C_{S1}$ is represent the total equivalent capacitor induced by three interdigital shape slit. In addition, the metal patch of section A is equivalent to $L_{P1}$ and the coupling effect between metal patch of section A and ground is equivalent to a shunt capacitor $C_{P1,}$ respectively. Because the section A and section C are symmetry about section B, the corresponding equivalent circuit model of section C is identical to section A. In section B, a parallel LC circuit consisting of $L_V$ and $C_{P2}$ is utilized to describe the parallel plates and via.

The EBG unit cell can be represented as equivalent parallel resonant LC circuit based on the simplification of 1-D equivalent circuit model depicted in Fig. 5 (b). When the surface wave between antenna elements propagates through the EBG structure, it will exhibit a resonant behavior with a resonance frequency $\omega_0 = 1/\sqrt{LC}$, where the L and C are the equivalent inductance and capacitance associated with the 1-D equivalent circuit model of EBG structure. Moreover, the effective permeability of EBG structure can be derived from the following equation [26]:

$$\mu_{\text{eff}} = 1 + \frac{F\omega_0}{\omega^{2-}\omega_0{}^2 + i\gamma} \tag{3}$$

where $\gamma$ is the dissipation factor, F is the fractional volume occupied by the metallic pattern in the unit cell and $\omega$ is the angular frequency of the surface wave. Conspicuously, the negative effective permeability can be attained when $\omega$ is below $\omega_{0.}$ Combining the above mentioned analysis and discussion, $\omega_0$ is immediately linked to the physical model of EBG structure and can be tunable. Hence, we can appropriately adjust the shape and the size of EBG structure for achieving negative effective permeability. As mentioned previously, the surface wave will be immensely suppressed when travelling in negative effective permeability media. Consequently, the coupling effect between antenna elements will be tremendously alleviated with the insertion of EBG structure.

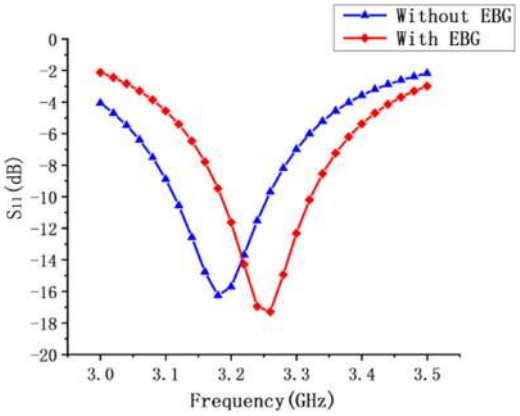


**FIGURE 6.** The reflection coefficient S11 of MIMO antenna with and without EBG structure.

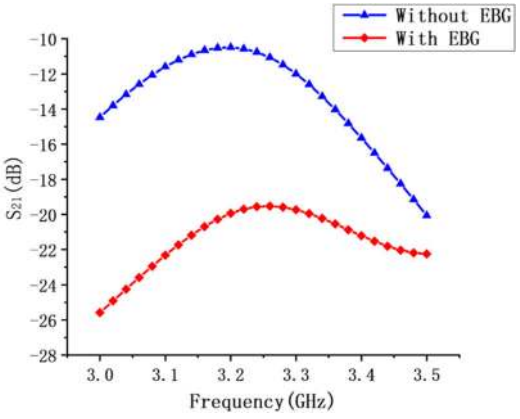


**FIGURE 7.** The transmission coefficient S21 of MIMO antenna with and without EBG structure.

In order to validate the feasibility of the decoupling concept analyzed in above, the simulated S parameter (reflection coefficient S11 and transmission coefficient S21) of MIMO antenna with and without EBG structure has been depicted in Fig. 6 and Fig. 7, respectively. It can be seen that antenna1 without EBG structure is working in 3.1 – 3.25 GHz with 4.8% impedance bandwidth. Comparing the reflection coefficient S11 between antenna 1 and antenna 2, the antenna working frequency has slightly shifted to high frequency after the insertion of EBG structure, attributed to the reason that the inevitable accompanying effect of EBG structure, which is not severe. In addition, the transmission coefficient S21 is below −10 dB at resonant frequency in antenna 1. Using antenna 1 as reference, the reduction of transmission coefficient has arrived at 9 dB after applying the EBG structure in antenna 2, which directly demonstrate that the aforementioned decoupling concept and theoretical analysis are reasonable. To give an intuitive illustration concerning about the working mechanism of EBG structure, the E-field and surface current of antenna elements

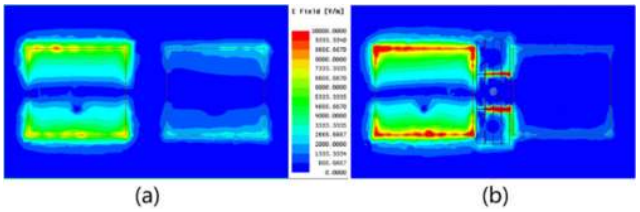


**FIGURE 8.** Simulated surface E-field distributions of H-plane coupled antenna at 3.25 GHz: without EBG structure (left) and with EBG structure (right).

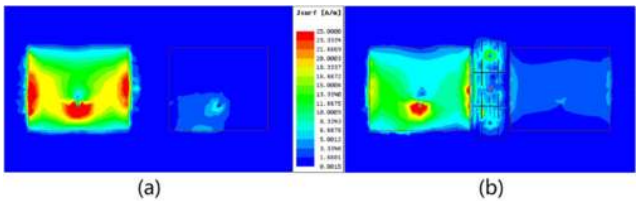


**FIGURE 9.** Simulated surface current distributions of H-plane coupled antenna at 3.25 GHz: without EBG structure (left) and with EBG structure (right).

have been studied. When patch 1 is excited while patch 2 is terminated by 50Ω match load. the surface E field distributions of MIMO antenna are shown in Fig. 8 with and without EBG structure. It is obvious that two elements without EBG structure are closely coupled through the nonradiation edge, which is known as H-plane coupling [27]. When loaded with EBG structure, the coupling E field is gradually attenuated in EBG structure patch and be densely constrained in interdigital shape slit. So the magnitude of excited E field in patch2 has been tremendously decreased compared with unloaded with EBG structure. Furthermore, it can be seen from Fig. 9 that the surface current flowing on patch 2 has been significantly suppressed after applying the EBG structure. Consequently, the decoupling concept of EBG has been confirmed that suppresses the propagation of surface wave between antenna elements.

The mutual coupling between antenna elements has been effectively alleviated in antenna 2 by blocking the propagation of surface wave. To further improve the isolation of antenna elements, the complementary split-ring resonators (CSRRs) have been introduced to reduce surface wave coupling in antenna 3 by guiding the wave propagation, which are placed in two sides of the ground adjacent to the nonradiation edge of the antenna element. CSRR is a pervasive metastructure which is extensively applied in MIMO decoupling. In previous research works, CSRRs are usually placed between antenna elements which play a role similar to EBG structure in hindering the propagation of surface wave [28]. The distinction between this work and previous research work is that CSRR is employed to steer the EM wave instead of blocking. The CSRR is the evolution of split-ring resonators according to the duality principle, whose physical model and corresponding equivalent circuit model are shown in Fig. 10. The CSRR also can be regarded as LC

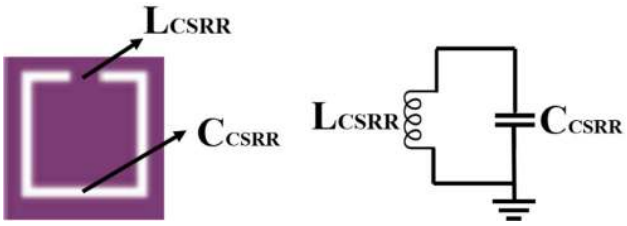


**FIGURE 10.** The physical model and corresponding equivalent circuit model of CSRR.

resonator like EBG structure, it resonance behavior is due to the induced electromotive force that generates a current that flows within the split ring gap and metallic connector, producing a balanced inductive-capacitive effect. Resonant frequency can be expressed as $\omega_0 = 1/\sqrt{LC}$, where L and C are the equivalent inductance and capacitance of CSRR respectively which are tunable by adjusting the physical shape and size of the CSRR. Furthermore, the effective permeability of CSRR can also be extracted from equation 3 mentioned in the previous section. When $\omega$ is larger than $\omega_{0,}$ the highly effective permeability of CSRR can be attained. A material with high permeability will guide and compress the magnetic lines in a compact space. Inspired by this, the CSRRs are utilized to steer the EM wave for pursuing the reduction of surface wave coupling. Hence, the total isolation of MIMO antenna elements will be improved.

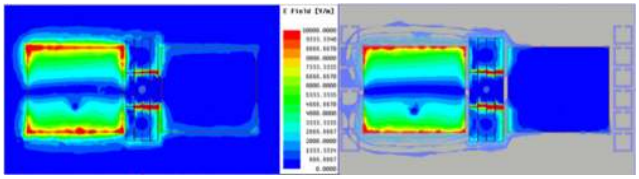

**FIGURE 11.** Simulated surface E-field distributions of H-plane coupled antenna at 3.25GHz: without CSRR structure (left) and with CSRR structure (right).

To visualize the wave steering effect of CSRR structure, the E field and surface current of MIMO antenna have been studied when patch 1 is excited while patch 2 is terminated with 50Ω match load. The surface E-field and current distributions of antenna with and without loading CSRR are exhibited in Fig. 11 and Fig. 12, respectively. After applying CSRR in antenna 3, it can be seen that the E field in patch 1 is attracted to the side adjacent the CSRR in coincide with the E filed decreasing in patch 2. Besides, Fig. 12 further reveals that both antenna top surface and ground currents have been steered to the area in the vicinity of CSRR, which supports our prediction and the wave steering characteristic of CSRR structure has been confirmed. Therefore, the mitigation of surface wave coupling between antenna elements is improved, which makes CSRR suitable for applying in the two sides of ground to enhance isolation characteristics. The simulated S parameters (reflection coefficient S11 and transmission coefficient S21 ) results with and without CSRR are exhibited in Fig. 13 and Fig. 14 for quantitative analysis.

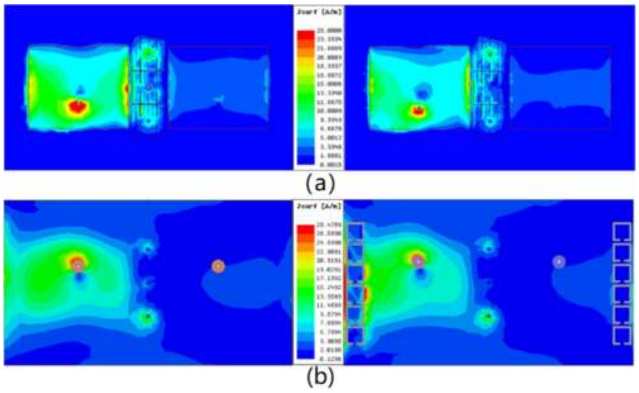


**FIGURE 12.** Simulated surface current distributions of H-plane coupled antenna at 3.25 GHz: without CSRR structure (left) and with CSRR structure (right).

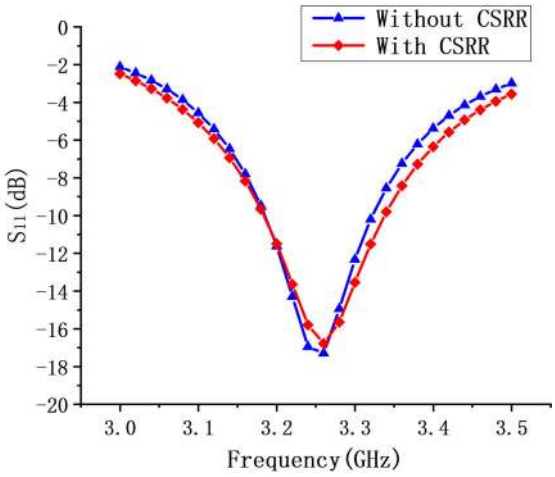


**FIGURE 13.** The reflection coefficient S11 of MIMO antenna with and without CSRR structure.

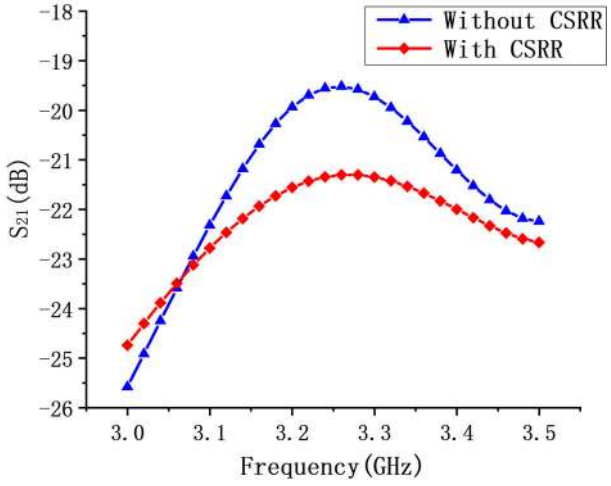


**FIGURE 14.** The transmission coefficient S21 of MIMO antenna with and without CSRR structure.

It can be seen that the reflection coefficient is almost unchanged after the introduction of CSRR which indicates that the parasitic effect of CSRR on impedance bandwidth can be negligible. While a slight reduction in transmission coefficient S21 is appearing from −19.5dB to −21.5 dB after applying CSRR, which is in accordance with the experimental phenomenon referred to surface E field and current distributions mentioned above.

To consolidate the isolation characteristics of antenna, in antenna 4, the H shape DGS is etched on the ground plane along the radiating edge of the antenna devoted to reverse part of the common ground current, which counteracts the partial coupling currents to increase isolation. The working mechanism of H shape DGS was elaborately analyzed in [29], so this paper only provides simulated S parameters. The reflection coefficient S11 and transmission coefficient S21 with and without H shape DGS are exhibited in Fig. 15 and Fig. 16, respectively. It can be seen from Fig. 15 that antenna impedance gets slightly worse after loaded with the H shape DGS, which is due to the inherent deficiency of H shape DGS. Meanwhile, the isolation of antenna elements has a slight improvement as described in Fig. 16.

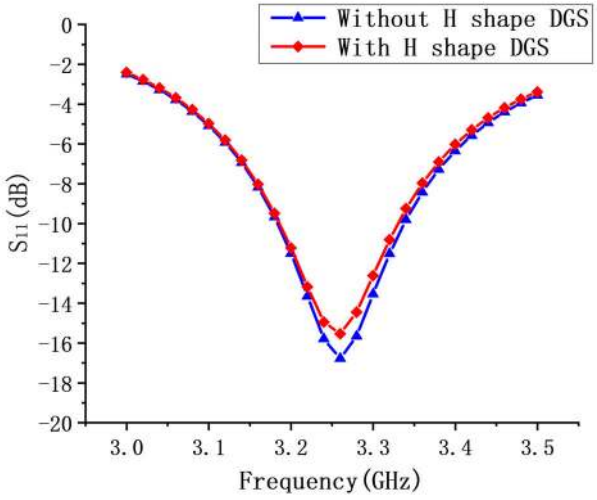


**FIGURE 15.** The reflection coefficient S11 of MIMO antenna with and without H shape DGS structure.

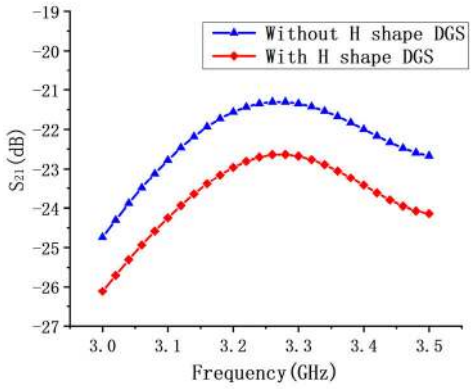


**FIGURE 16.** The transmission coefficient S21 of MIMO antenna with and without H shape DGS structure.

### *D. PARAMETER STUDYING*

To get the optimized performance of proposed MIMO antenna and make better sense of design principle, a set of parametric study has been carried out. The length of

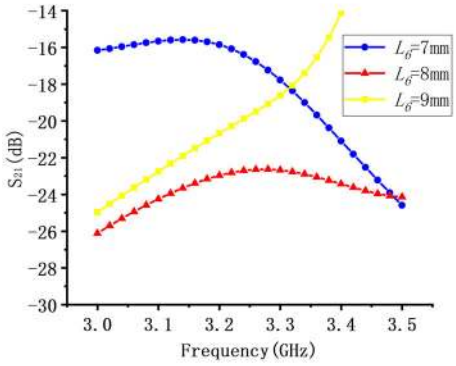


**FIGURE 17.** The effect of mushroom patch length on antenna transmission coefficient S21.

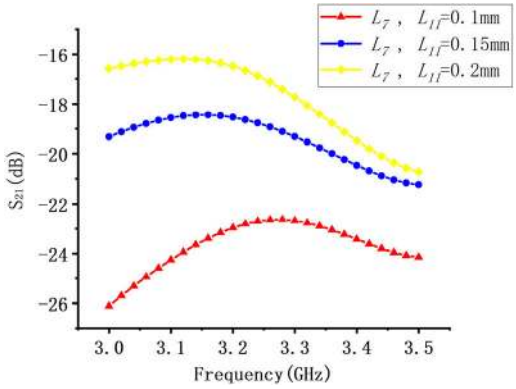


**FIGURE 18.** The effect of interdigital slit width on antenna transmission coefficient S21.

square mushroom patch and the width of interdigital shape slit are mainly investigated to show their effect on antenna performance, while only one geometrical parameter is varied each time and the rest are fixed. The simulated transmission coefficient S21 with different values of $L_6$, $L_7$ and $L_{11}$ are shown in Fig. 17 and Fig. 18, respectively. The influences of the length of square mushroom patch are observed to have a significant effect on antenna isolation characteristic in figure 17, which is due to the length of mushroom patch associated with the equivalent inductance and capacitance of EBG mentioned in above.

By considering the best performance of isolation, the optimal length of square mushroom patch is chosen as 8mm. Fig 18 depicts the effect of different interdigital shape slit width on antenna isolation characteristic. As it can be observed clearly, the transmission coefficient is extremely sensitive to the variation of L7 and L11, which is in accordance with the surface E field distributions exhibited in Fig. 8 that the surface E field is concentrated in interdigital slits. Considering the fabrication accuracy in subsequent step and performance of isolation, the optimal value of L7 and L11 is chosen as 0.1mm. The rest parameter analysis procedure is similar as above, which is not listed in this section for brevity.

**FIGURE 19.** The prototype of proposed antenna: top view (left) and bottom view (right).

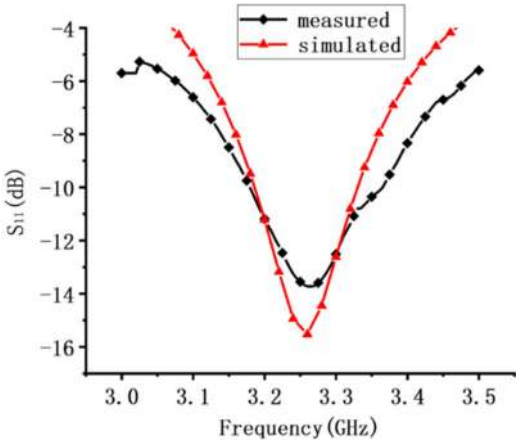


**FIGURE 20.** Comparison of the simulated and measured reflection coefficient.

## III. EXPERIMENTAL RESULTS

In order to validate the feasibility of the proposed decoupling concept, the designed MIMO antenna was fabricated and measured. The proposed antenna prototype is shown in Fig. 19 with top and bottom view, which is fabricated by using standard printed circuit board (PCB) technology with the size of 40mm∗70mm∗3mm and the thickness of copper 0.035mm. Besides, antenna elements are fed through two 50Ω SMA connector. The reflection coefficient and mutual coupling of fabricated MIMO antenna are measured using Agilent E8362B two port network analyzer, while the gain and radiation pattern are measured in anechoic environment with one port excited and another port terminated with 50Ω match load, using standard-gain antenna as a reference. The comparison of simulated and measured results of reflection coefficient and transmission coefficient are exhibited in Fig. 20 and Fig 21, respectively. From the result comparison, it can be seen apparently that the measured reflection coefficient result has a great agreement with the simulated. Nevertheless, it remains some discrepancy in transmission coefficient between simulated and measured that the measured result exhibits sharply decreasing tendency in the out of work band compared with simulated, which can be attributed to the cumulative effect of fabrication (in fabrication process, the copper layers have the thickness of 0.035mm and metallic vias are employed to substitute the metal pins of EBG structure in simulation ), assembly (the insertion of SMA connector), alignment errors of CSRR and EBG structure. According to the parametric studying in the previous section,

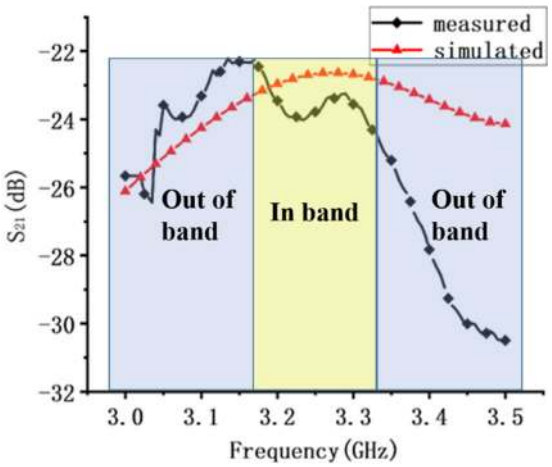


**FIGURE 21.** Comparison of the simulated and measured transmission coefficient.

which indicates that the transmission coefficient is extremely sensitive to the size of EBG structure. Thus, the metal loss and fabrication errors may promote the evanescence of surface wave in the out of work band, which will accelerate the original decreasing tendency of transmission coefficient in simulation. Fortunately, the measurement result shows that the mismatch between simulated and measured about transmission coefficient is mainly concentrated in the range out of antenna work band and their difference is less than 2 dB in band, which is imperfect but acceptable.

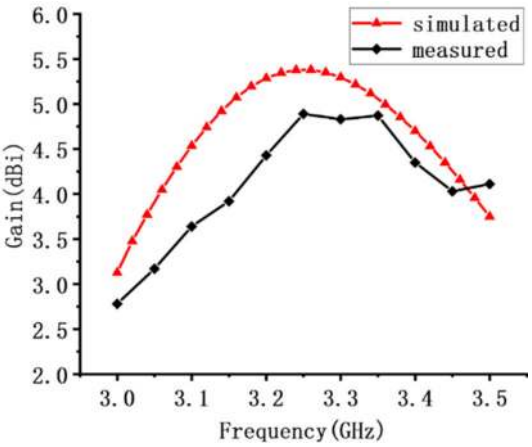


**FIGURE 22.** Comparison of the simulated and measured antenna gain.

Fig. 22 illustrates the comparison of simulated and measured results of antenna gain, where the measured maximum gain reaches 4.9dBi at 3.25 GHz. It can be seen clearly that the measured result is slightly lower than the simulated, which is due to the deficiency of fabrication and the insertion loss of SMA connector. But the gain variation tendency between the simulated and measured has a great agreement. The comparison of simulated and measured normalized radiation patterns in XOZ and YOZ plane is shown in Fig. 23, where the measured result is in accordance with the simulated. Conspicuously, an oblique of radiation pattern in YOZ plane is appearing and the gain peak point is located in theta = 30°. According to the cavity theory, the near E-fields of a microstrip patch antenna are mostly perpendicular to its patch. Consequently, the peak gain of microstrip patch antenna is normally appear in theta = 0°. Hence, the oblique experimental phenomenon concerning about radiation pattern in YOZ plane immediately validate the guiding wave characteristic of CSRR structure, which indicates that space correlation of antenna elements is reduced.

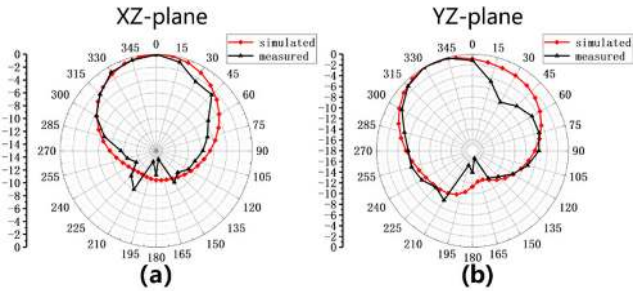


**FIGURE 23.** Comparison of simulated and measured normalized radiation pattern. (a) XOZ plane. (b) YOZ plane.

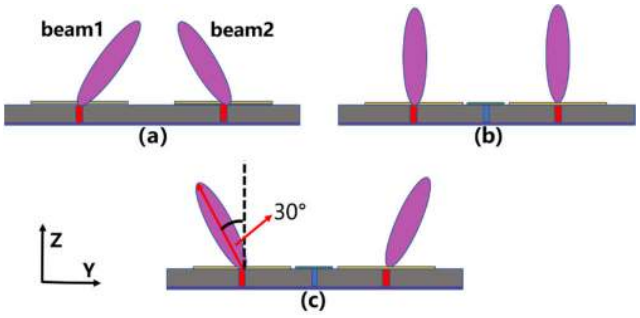


**FIGURE 24.** States of antenna beam in design procedures. (a) without decoupling structure (b) with EBG structure (c) with EBG and CSRR structure.

## IV. CONCLUSIONS

In this paper, a two element MIMO antenna has been developed. The antenna isolation characteristic enhancing procedures and corresponding decoupling concept have been meticulously analyzed. A decoupling mechanism concerning about steering and suppressing surface wave propagation simultaneously was exploited for enhancing antenna isolation characteristic. Furthermore, H shape DGS was introduced to strengthen the total decoupling effect. The briefly schematic illustration is depicted in Fig. 24, which illustrates the three states of antenna beams in relevant design procedures. A detailed comparison between other similar decoupling methods referred to microstrip patch antenna on some key indicators is shown in Table 2. With reference to the table, the proposed antenna yields acceptable coupling suppression, relatively compact planar dimension and low profile simultaneously. Besides, only a substrate layer is employed in this work, which is a generalized technique for two port MIMO

**TABLE 2. Comparison with previous works.**

| Reference | [18] | [24] | [27] | [28] | This work |
|---|---|---|---|---|---|
| **Antenna type** | MPA | MPA | MPA | MPA | MPA |
| **Freq (GHz)** | 4.9 | 5.8 | 3.51 | 5.00 | 3.25 |
| **Method** | ELC | UC-EBG | MS | SC-SRR | EBG CSRR HDGS |
| **Coupling suppression (dB)** | 23 | 10 | 41 | 10 | 12 |
| **Electrical dimension ($\lambda_0$)** | 0.42*0.69 | 1.51*1.51 | 1.17*1.47 | 1.3*1.0 | 0.43*0.76 |
| **Profile height ($\lambda_0$)** | 0.18 | 0.049 | 0.2 | 0.021 | 0.032 |
| **Edge-to-Edge spacing ($\lambda_0$)** | 0.017 | 0.5 | 0.023 | 0.25 | 0.11 |
| **Substrate Layers** | 2 | 2 | 2 | 1 | 1 |

*$\lambda_0$ is free space wavelength at center frequency

and can be easily extended for large MIMO systems with low cost.

## REFERENCES

[1] G. J. Foschini, "Layered space-time architecture for wireless communication in a fading environment when using multi-element antennas," *Bell Labs Tech. J.*, vol. 1, no. 2, pp. 41–59, Aug. 1996.
[2] X. Li and Z.-P. Nie, "Mutual coupling effects on the performance of MIMO wireless channels," *IEEE Antennas Wireless Propag. Lett.*, vol. 3, pp. 344–347, 2004.
[3] S. Zhang and G. F. Pedersen, "Mutual coupling reduction for UWB MIMO antennas with a wideband neutralization line," *IEEE Antennas Wireless Propag. Lett.*, vol. 15, pp. 166–169, 2016.
[4] X.-J. Zou, G.-M. Wang, Y.-W. Wang, and H.-P. Li, "An efficient decoupling network between feeding points for multielement linear arrays," *IEEE Trans. Antennas Propag.*, vol. 67, no. 5, pp. 3101–3108, May 2019.
[5] A. Ghalib and M. S. Sharawi, "TCM analysis of defected ground structures for MIMO antenna designs in mobile terminals," *IEEE Access*, vol. 5, pp. 19680–19692, 2017.
[6] C. Kumar, M. I. Pasha, and D. Guha, "Defected ground structure integrated microstrip array antenna for improved radiation properties," *IEEE Antennas Wireless Propag. Lett.*, vol. 16, pp. 310–312, 2017.
[7] K. Wei, J.-Y. Li, L. Wang, Z.-J. Xing, and R. Xu, "Mutual coupling reduction by novel fractal defected ground structure bandgap filter," *IEEE Trans. Antennas Propag.*, vol. 64, no. 10, pp. 4328–4335, Oct. 2016.
[8] M.-Y. Li, Y.-L. Ban, Z.-Q. Xu, G. Wu, C.-Y.-D. Sim, K. Kang, and Z.-F. Yu, "Eight-port orthogonally dual-polarized antenna array for 5G smartphone applications," *IEEE Trans. Antennas Propag.*, vol. 64, no. 9, pp. 3820–3830, Sep. 2016.
[9] M.-Y. Li, Z.-Q. Xu, Y.-L. Ban, C.-Y.-D. Sim, and Z.-F. Yu, "Eight-port orthogonally dual-polarised MIMO antennas using loop structures for 5G smartphone," *IET Microw., Antennas Propag.*, vol. 11, no. 12, pp. 1810–1816, Sep. 2017.
[10] C. F. Ding, X. Y. Zhang, C.-D. Xue, and C.-Y.-D. Sim, "Novel pattern-diversity-based decoupling method and its application to multielement MIMO antenna," *IEEE Trans. Antennas Propag.*, vol. 66, no. 10, pp. 4976–4985, Oct. 2018.
[11] K. Saurav, N. K. Mallat, and Y. M. M. Antar, "A three-port polarization and pattern diversity ring antenna," *IEEE Antennas Wireless Propag. Lett.*, vol. 17, no. 7, pp. 1324–1328, Jul. 2018.
[12] R.-H. Fan, B. Xiong, R.-W. Peng, and M. Wang, "Constructing metastructures with broadband electromagnetic functionality," *Adv. Mater.*, 2019, Art. no. 1904646, doi: 10.1002/adma.201904646.
[13] S. Sun, Q. He, J. Hao, S. Xiao, and L. Zhou, "Electromagnetic metasurfaces: Physics and applications," *Adv. Opt. Photon.*, vol. 11, no. 2, pp. 380–479, 2019.
[14] X. Tan, W. Wang, Y. Wu, Y. Liu, and A. A. Kishk, "Enhancing isolation in dual-band meander-line multiple antenna by employing split EBG structure," *IEEE Trans. Antennas Propag.*, vol. 67, no. 4, pp. 2769–2774, Apr. 2019.
[15] M. Li, B. G. Zhong, and S. W. Cheung, "Isolation enhancement for MIMO patch antennas using near-field resonators as coupling-mode transducers," *IEEE Trans. Antennas Propag.*, vol. 67, no. 2, pp. 755–764, Feb. 2019.
[16] J. Barrett. (Feb. 2017). *5G Spectrum Bands*. [Online]. Available: https://gsacom.com/5g-spectrum-bands/
[17] W. Yang, Y. Zhang, W. Che, M. Xun, Q. Xue, G. Shen, and W. Feng, "A simple, compact filtering patch antenna based on mode analysis with wide out-of-band suppression," *IEEE Trans. Antennas Propag.*, vol. 67, no. 10, pp. 6244–6253, Oct. 2019.
[18] L. Si, H. Jiang, X. Lv, and J. Ding, "Broadband extremely close-spaced 5G MIMO antenna with mutual coupling reduction using metamaterial-inspired superstrate," *Opt. Express*, vol. 27, no. 3, pp. 3472–3482, 2019.
[19] M. M. Bait-Suwailam, M. S. Boybay, and O. M. Ramahi, "Electromagnetic coupling reduction in high-profile monopole antennas using single-negative magnetic metamaterials for MIMO applications," *IEEE Trans. Antennas Propag.*, vol. 58, no. 9, pp. 2894–2902, Sep. 2010.
[20] F.-M. Yang, L. Peng, X. Liao, K.-S. Mo, X. Jiang, and S.-M. Li, "Coupling reduction for a wideband circularly polarized conformal array antenna with a single-negative structure," *IEEE Antennas Wireless Propag. Lett.*, vol. 18, no. 5, pp. 991–995, May 2019.
[21] T. D. Karamanos, A. I. Dimitriadis, and N. V. Kantartzis, "Compact double-negative metamaterials based on electric and magnetic resonators," *IEEE Antennas Wireless Propag. Lett.*, vol. 11, pp. 480–483, 2012.
[22] A. Grande, J. A. Pereda, O. Gonzalez, and N. Vegas, "On the equivalence of several FDTD formulations for modeling electromagnetic wave propagation in double-negative metamaterials," *IEEE Antennas Wireless Propag. Lett.*, vol. 6, pp. 324–327, 2007.
[23] Y. Liu, X. Yang, Y. Jia, and Y. J. Guo, "A low correlation and mutual coupling MIMO antenna," *IEEE Access*, vol. 7, pp. 127384–127392, 2019.
[24] H. S. Farahani, M. Veysi, M. Kamyab, and A. Tadjalli, "Mutual coupling reduction in patch antenna arrays using a UC-EBG superstrate," *IEEE Antennas Wireless Propag. Lett.*, vol. 9, pp. 57–59, 2010.
[25] P. Sambandam, M. Kanagasabai, S. Ramadoss, R. Natarajan, M. G. N. Alsath, S. Shanmuganathan, M. Sindhadevi, and S. K. Palaniswamy, "Compact monopole antenna backed with fork-slotted EBG for wearable applications," *IEEE Antennas Wireless Propag. Lett.*, vol. 19, no. 2, pp. 228–232, Feb. 2020, doi: 10.1109/LAWP.2019.2955706.
[26] Z. Liu, J. Wang, S. Qu, J. Zhang, H. Ma, Z. Xu, and A. Zhang, "Enhancing isolation of antenna arrays by simultaneously blocking and guiding magnetic field lines using magnetic metamaterials," *Appl. Phys. Lett.*, vol. 109, no. 15, pp. 153505-1–153505-5, Oct. 2016.
[27] H. Luan, C. Chen, W. Chen, L. Zhou, H. Zhang, and Z. Zhang, "Mutual coupling reduction of closely E/H-plane coupled antennas through metasurfaces," *IEEE Antennas Wireless Propag. Lett.*, vol. 18, no. 10, pp. 1996–2000, Oct. 2019.

[28] M. M. Bait-Suwailam, O. F. Siddiqui, and O. M. Ramahi, "Mutual coupling reduction between microstrip patch antennas using slotted-complementary split-ring resonators," *IEEE Antennas Wireless Propag. Lett.*, vol. 9, pp. 876–878, 2010.
[29] Z. Niu, H. Zhang, Q. Chen, and T. Zhong, "Isolation enhancement in closely coupled dual-band MIMO patch antennas," *IEEE Antennas Wireless Propag. Lett.*, vol. 18, no. 8, pp. 1686–1690, Aug. 2019.

**ZHUO YANG** was born in Jingmen, China, in 1995. He received the B.S. degree in photoelectric information engineering from Hubei Normal University, Huangshi, China, in 2017. He is currently pursuing the M.S. degree in microwave and antenna technology with Jimei University. He has recently authored or coauthored two conference papers. His current research interests include wideband patch antennas, metasurfaces, and MIMO decoupling.

**JUN XIAO** received the B.S. and M.S. degrees from the Harbin Institute of Technology, Harbin, China, in 2008 and 2011, respectively, and the Ph.D. degree from the Beijing University of Posts and Telecommunications, Beijing, China, in 2019. Then, he joined the School of Information Engineering, Jimei University, Xiamen, China, as an Associate Professor. His current research interests include millimeter-wave antennas and THz antennas.

**QIUBO YE** (Senior Member, IEEE) received the bachelor's degree from the University of Manitoba, Canada, the master's degree from North China Electric Power University, and the Ph.D. degree from the Hefei University of Technology, China, all in electrical engineering. He was a Research Scientist/Project Leader of the Communications Research Centre Canada, a Visiting Assistant Professor at the Rose-Hulman Institute of Technology, USA, and a Research and Development Engineer with Zeland Software, Inc., USA. He was an Adjunct Research Professor with the Department of Electronics, Carleton University, Canada. He is currently a Chair Professor with the School of Information Engineering, Jimei University, Xiamen, China. He has published books, book chapters, and more than 80 research articles. His research interests include computational electromagnetics, antennas, EMC/EMI, wave propagation, wireless communication, and the applications of AI in communications. He has received the Outstanding Engineer Award from the IEEE Ottawa and other awards for his outstanding performance as the Chair of the IEEE Ottawa AP/MTT Joint Chapter. He was the General Chair of the IASTED International Conference on Wireless Communication, in 2011, and the IEEE International Symposium on EMC, in 2016.